

# A 2-Helix Small Protein Labeled with $^{68}\text{Ga}$ for PET Imaging of *HER2* Expression

Gang Ren<sup>1</sup>, Rong Zhang<sup>2</sup>, Zhe Liu<sup>1</sup>, Jack M. Webster<sup>2</sup>, Zheng Miao<sup>1</sup>, Sanjiv S. Gambhir<sup>1</sup>, Faisal A. Syud<sup>2</sup>, and Zhen Cheng<sup>1</sup>

<sup>1</sup>Molecular Imaging Program at Stanford (MIPS), Department of Radiology and Bio-X Program, Stanford University, Stanford, California; and <sup>2</sup>Global Research, General Electric Co., Niskayuna, New York

Affibody molecules are a class of scaffold proteins being developed into a generalizable approach to targeting tumors. Many 3-helix-based Affibody proteins have shown excellent in vivo properties for tumor imaging and therapy. By truncating one  $\alpha$ -helix that is not responsible for receptor recognition in the Affibody and maturing the protein affinity through synthetic strategies, we have successfully identified in our previous research several small 2-helix proteins with excellent binding affinities to human epidermal growth factor receptor type 2 (*HER2*). With preferential properties such as faster blood clearance and tumor accumulation, lower immunogenic potential, and facile and economically viable synthetic schemes, we hypothesized that these 2-helix protein binders could become excellent molecular imaging probes for monitoring *HER2* expression and modulation.

**Methods:** In this study, a 2-helix small protein, MUT-DS, was chemically modified with a metal chelator, 1,4,7,10-tetraazacyclododecane-1,4,7,10-tetraacetic acid (DOTA). DOTA-MUT-DS was then site-specifically radiolabeled with an important PET radionuclide,  $^{68}\text{Ga}$ . The resulting radiolabeled anti-*HER2* 2-helix molecule was further evaluated as a potential molecular probe for small-animal PET *HER2* imaging in a SKOV3 tumor mouse model. **Results:** The 2-helix DOTA-MUT-DS showed high *HER2*-binding affinity (dissociation constant, 4.76 nM). The radiolabeled probe displayed high stability in mouse serum and specificity toward *HER2* in cell cultures. Biodistribution and small-animal PET studies further showed that  $^{68}\text{Ga}$ -DOTA-MUT-DS had rapid and high SKOV3 tumor accumulation and quick clearance from normal organs. The specificity of  $^{68}\text{Ga}$ -DOTA-MUT-DS for SKOV3 tumors was confirmed by monitoring modulation of *HER2* protein on treatment of tumor mice with heat shock protein 90 inhibitor 17-*N,N*-dimethyl ethylene diamine-geldanamycin in vivo. **Conclusion:** This proof-of-concept research clearly demonstrated that synthetic 2-helix  $^{68}\text{Ga}$ -DOTA-MUT-DS is a promising PET probe for imaging *HER2* expression in vivo. The Affibody-derived small 2-helix protein scaffold has great potential for developing targeting agents for a variety of tumor-associated biomarkers.

**Key Words:** *HER2*; Affibody; PET; imaging;  $^{68}\text{Ga}$

**J Nucl Med** 2009; 50:1492–1499

DOI: 10.2967/jnumed.109.064287

Affibody molecules (Affibody AB), nonimmunogenic 3-helix scaffold-based small proteins (~7 kDa), have recently drawn much attention for developing affinity ligands against a variety of molecular targets (1,2). Affibody molecules were derived from one of the IgG-binding domains of staphylococcal protein A, and they are composed of a relatively small engineered nonimmunoglobulin protein scaffold with 58 amino acid residues and a 3- $\alpha$ -helical bundle scaffold structure. Affibody molecule libraries can be easily constructed by randomization of 13 amino acid residues in helices 1 and 2 of the 3-helix bundle protein (Fig. 1A). Thus, Affibody binders with high affinity and specificity against a wide variety of desired targets, such as human epidermal growth factor receptor type 2 (*HER2*) (3,4), epidermal growth factor receptor (5,6), human serum albumin (7), interleukin-2 receptor alpha/CD25 (8), transcription factor c-Jun (9), Alzheimer amyloid  $\beta$ -peptides (10), and HIV-1 gp120 (11), have been quickly identified and selected using phage-display library technology and affinity maturation.

*HER2*-binding 3-helix Affibody molecules have been extensively studied and subsequently radiolabeled with a variety of radioisotopes, such as  $^{18}\text{F}$ ,  $^{68}\text{Ga}$ ,  $^{64}\text{Cu}$ ,  $^{99\text{m}}\text{Tc}$ ,  $^{111}\text{In}$ ,  $^{90}\text{Y}$ , and  $^{177}\text{Lu}$ , for *HER2*-targeted tumor imaging and radiotherapy (12–19). These studies have clearly demonstrated the potential use of 3-helix protein scaffold-based Affibody molecules in clinical cancer management. Moreover, the rapid and exciting progress in research on Affibody proteins has encouraged more studies to use many other protein scaffolds for molecular probe development.

Our preliminary studies found that of the various anti-*HER2* Affibody protein constructs available (monomeric [~7 kDa] vs. dimeric [~14 kDa]), the smaller one performed substantially better in vivo in terms of tumor uptake and clearance (18). Additional advantages expected for smaller protein constructs include the possibility of facile synthetic generation and easier library generation for screening, economic viability, and potentially lower immunogenic potential. Because the binding domain of the Affibody molecules localizes only in the  $\alpha$ -helices 1 and 2 bundle of Affibody, helix 3 is not involved in receptor

Received Mar. 16, 2009; revision accepted May 21, 2009.

For correspondence or reprints contact: Zhen Cheng, Molecular Imaging Program at Stanford, Department of Radiology, Bio-X Program, 1201 Welch Rd., Lucas Expansion, P020A, Stanford University, Stanford, CA 94305.

E-mail: zcheng@stanford.edu

COPYRIGHT © 2009 by the Society of Nuclear Medicine, Inc.

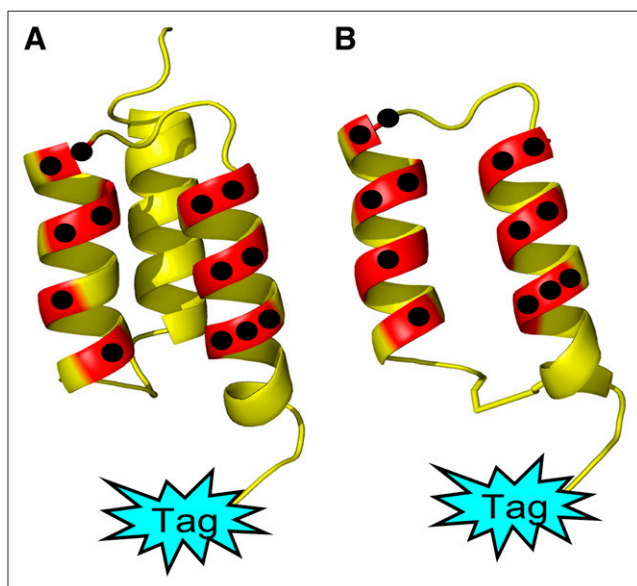


**FIGURE 1.** Three-helix Affibody and 2-helix protein scaffold-based PET probes for *HER2* imaging. Black dots and red regions indicate amino acid residues responsible for receptor binding.

recognition and contributes only to stabilizing the protein; therefore, in our recent research, helix 3 was truncated to generate a class of small proteins consisting of 2  $\alpha$ -helix bundles of Affibody (Fig. 1B). In addition, several sequence mutations and synthetic strategies to optimize the affinity of 2-helix against *HER2* have been developed. More than thirty 2-helix small protein constructs were synthesized. Several constrained 2-helix constructs including MUT-DS (sequence: [homoC]NKEMRNRYWEAALDPNLNNQQRKAKIRSIYDDP[homoC]-NH<sub>2</sub>, with a disulfide bridge being formed between 2 homocysteines) with high *HER2*-binding affinity (low nM) were successfully identified (20).

In this research, we hypothesized that the small 2-helix protein scaffold has great potential to serve as a unique platform for developing agents for *in vivo* targeting of cancer-associated biomarkers, and specifically for targeting of *HER2*. Thus, a 1,4,7,10-tetraazacyclododecane-1,4,7,10-tetraacetic acid (DOTA)-conjugated MUT-DS analog, DOTA-MUT-DS (sequence: DOTA-VENK[homoC]NKEMRNRYWEAALDPNLNNQ QKRAKIRSIYDDP[homoC]-NH<sub>2</sub>, with a disulfide bridge being formed between 2 homocysteines) was then synthesized and radiolabeled with an important PET radionuclide, <sup>68</sup>Ga (half-life, 67.6 min; maximum energy [ $\beta^+$ ], 1,899 keV;  $\beta^+$  decay, 89%). The *in vitro* and *in vivo* biologic profiles of this <sup>68</sup>Ga-labeled anti-*HER2* 2-helix small protein were further evaluated in SKOV3 cell lines with high *HER2* expression and nude mice bearing subcutaneous SKOV3 tumors. Finally, the ability of 2-helix <sup>68</sup>Ga-DOTA-MUT-DS to image *HER2* expression in living mice was also evaluated using small-animal PET.

## MATERIALS AND METHODS

### General

The Affibody molecule Z<sub>HER2:477</sub>, an anti-*HER2* imaging agent, was purchased from Affibody AB. DOTA-tri-*tert*-butyl ester was obtained from Macrocylics Inc. 17-*N,N*-dimethyl ethylene diamine-geldanamycin (17-DMAG) was obtained from Invivo-Gen. (*S*)-2-(Fmoc-amino)-4-tritylsulfanyl-butyric acid [Fmoc-HomoCys(Trt)-OH] was purchased from Bachem Bioscience, Inc. Trifluoroacetic acid, *O*-benzotriazole-*N,N,N',N'*-tetramethyluronium hexafluorophosphate, 4-(2',4'-dimethoxyphenyl-Fmoc-aminomethyl)-phenoxy resin (rink amide resin, low substitution, 100–200 mesh, 1% divinylbenzene, 0.2 mmol/g), and all other *N*- $\alpha$ -Fmoc-protected amino acids were purchased from Advanced Chemtech. Dimethylformamide and methylene chloride were from Fisher Scientific. Piperidine (20%) in dimethylformamide and 0.4 M *N*-methylmorpholine in dimethylformamide were from Protein Technologies Inc. Pyridine, acetic anhydride, acetic acid, and anhydrous ether were from J.T. Baker. High-performance liquid chromatography (HPLC)-grade acetonitrile (CH<sub>3</sub>CN) and 18-m $\Omega$  water (Millipore) were used for peptide purification. Triisopropylsilane, 1,2-ethanedithiol, and all other standard synthesis reagents were purchased from Sigma-Aldrich Chemical Co. The radionuclide, <sup>68</sup>Ga, was eluted with 0.1N HCl from a <sup>68</sup>Ge/<sup>68</sup>Ga generator (Cyclotron). All other general materials (e.g., cell lines and mice) and instruments (e.g., reverse-phase HPLC, radioactive dose calibrator, and mass spectrometer) were the same as previously reported (18).

### Synthesis of DOTA-MUT-DS

The cyclic 2-helix small protein DOTA-MUT-DS was synthesized using standard solid-phase Fmoc chemistry and rink amide resin LS (substitution of 0.2 mmol/g on a 40- $\mu$ mol scale). The linear peptide was first synthesized using a Prelude peptide synthesizer (Protein Technologies Inc.) and purified by HPLC. Then, the linear peptide was cyclized by I<sub>2</sub> oxidation of the 2 homocysteines to form a disulfide bridge. Briefly, the peptide (1–3 mg) dissolved in 1 mL of 50% acetic acid was diluted with 9 mL of 1N HCl, followed by the immediate addition of 0.1 M I<sub>2</sub> in 50% acetic acid. After 30 min of stirring, the reaction was quenched by the addition of 1 M aqueous sodium thiosulfate dropwise. Both crude linear and cyclized peptides were purified by reverse-phase preparative HPLC with a protein-and-peptide C4 column (Vydac). The mobile phase was solvent A, 0.05% trifluoroacetic acid/H<sub>2</sub>O (v/v), and solvent B, 0.05% trifluoroacetic acid/acetonitrile (v/v). The gradient condition was 20%–35% B over 45 min. The flow rate was typically 25 mL/min. Fractions containing the product were collected and lyophilized. The identity of the target peptides was confirmed by matrix-assisted laser desorption/ionization time-of-flight mass spectrometry (Voyager-DE RP Biospectrometer; PerSeptive Biosystems) or electrospray ionization time-of-flight mass spectrometry (JMS-T100LC; JEOL Ltd.).

### *In Vitro* Analysis of 2-Helix Small Protein

The *HER2*-binding affinity of DOTA-MUT-DS was measured *in vitro* using surface plasmon resonance detection on a Biacore 3000 instrument (GE Healthcare) according to the method reported previously (18).

### <sup>68</sup>Ga Radiolabeling of 2-Helix Small Protein

The DOTA-MUT-DS was radiolabeled with <sup>68</sup>Ga by the addition of 29.6 MBq (0.8 mCi) of <sup>68</sup>GaCl<sub>3</sub> (1  $\mu$ g of protein per 1.97

MBq of  $^{68}\text{Ga}$  in 0.1N  $\text{NH}_4\text{OAc}$  (pH 4.5) buffer followed by a 20-min incubation at  $75^\circ\text{C}$ . The radiolabeled complex was then purified by analytic radio-HPLC. The flow rate was 1 mL/min, with the mobile phase being 95% solvent A and 5% solvent B from 0 to 3 min, 35% solvent A and 65% solvent B at 33 min, and 15% solvent A and 85% solvent B from 33 to 36 min. This solvent composition was then maintained for another 3 min (36–39 min), and the initial solvent composition was resumed by 42 min. Purified radiolabeled small protein was dried by a rotary evaporator and analyzed by radio-HPLC. The radiolabeled compound was reconstituted in phosphate-buffered saline and passed through a 0.22- $\mu\text{m}$  Millipore filter into a sterile vial for in vitro and animal experiments.

### Serum Stability

$^{68}\text{Ga}$ -DOTA-MUT-DS (740 kBq) in 50  $\mu\text{L}$  of phosphate-buffered saline was added to 500  $\mu\text{L}$  of mouse serum (Sigma). After incubation at  $37^\circ\text{C}$  for 40 min, the solution was filtered through a NanoSep device (10K; Pall Corp.). The filtrate was then injected into the radio-HPLC column under conditions identical to those used for analyzing the original radiolabeled compound. The fractions eluted from HPLC were collected into plastic tubes every 30 s. The radioactivity of each tube was counted by a  $\gamma$ -counter (model 1470; PerkinElmer), and the radio-HPLC chromatogram was plotted using Origin, version 6.0 (MicroCal).

### Cell Assays

SKOV3 cells were cultured in McCoy 5 medium supplemented with 10% fetal bovine serum and 1% penicillin–streptomycin (Invitrogen Life Technologies). The cells were maintained in a humidified atmosphere of 5%  $\text{CO}_2$  at  $37^\circ\text{C}$ , with the medium changed every other day. A 70%–80% confluent monolayer was detached by 0.1% trypsin and dissociated into a single-cell suspension for further cell culture.

The in vitro cell uptake assays of the  $^{68}\text{Ga}$ -DOTA-MUT-DS were performed with the SKOV3 cells as previously described (18). Briefly, cells were seeded at a density of 0.15 million per well in 12-well tissue culture plates and allowed to attach overnight. After 2 washes with the serum-free McCoy 5 medium, the cells were incubated at  $37^\circ\text{C}$  for 0.5–2 h with  $^{68}\text{Ga}$ -DOTA-MUT-DS (6.29 kBq [0.17  $\mu\text{Ci}$ ], 10 ng) in 0.5 mL of serum-free medium. The nonspecific binding of the probes with SKOV3 cells was then determined by coincubation with nonradioactive  $Z_{\text{HER2}:477}$  protein (1  $\mu\text{g}$  of  $Z_{\text{HER2}:477}$  was added to each sample for  $^{68}\text{Ga}$ -DOTA-MUT-DS; final concentration was 0.28  $\mu\text{M}$ ). The cells were rinsed 3 times with 0.01 M phosphate-buffered saline (pH 7.4) and 0.2% bovine serum albumin and lysed in 0.3 mL of 0.5 M NaOH at room temperature for 5 min, and the radioactivity of the cells was counted using a PerkinElmer 1470 automatic  $\gamma$ -counter. The uptake (counts/min) was normalized to percentage of binding for analysis using Prism, version 5.0 (GraphPad).

### Biodistribution Studies

All animal studies were performed in compliance with federal and local institutional rules for the conduct of animal experimentation. Approximately  $3 \times 10^6$  SKOV3 cells suspended in phosphate-buffered saline were implanted subcutaneously in the right upper shoulders of nude mice. Tumors were allowed to grow to around 50  $\text{mm}^3$  (3–4 wk), and the tumor-bearing mice were subjected to in vivo biodistribution and imaging studies.

For biodistribution studies, the SKOV3 tumor-bearing mice ( $n = 3$  for each group) were injected with radiolabeled Affibody

proteins (0.296 MBq [8  $\mu\text{Ci}$ ], 0.415–0.515  $\mu\text{g}$ ) through the tail vein and sacrificed at different time points from 30 min to 2 h after injection. Tumor and normal tissues of interest were excised and weighed, and their radioactivity was measured in a  $\gamma$ -counter. The radioactivity uptake in the tumor and normal tissues was expressed as a percentage of the injected radioactive dose per gram of tissue (%ID/g). To test the in vivo *HER2*-targeting specificity, nude mice bearing SKOV3 tumor ( $n = 3$  for each group) were treated with a heat shock protein 90 (hsp90) inhibitor, 17-DMAG. A dose of 50 mg/kg was dissolved in phosphate-buffered saline and intraperitoneally injected into the abdomen of the mice 3 times (every 8 h until the initiation of image acquisition). The mice were then injected with  $^{68}\text{Ga}$ -DOTA-MUT-DS, and biodistribution studies were performed at 0.5, 1, and 2 h after injection.

### Small-Animal PET

PET of tumor-bearing mice was performed on a microPET R4 rodent model scanner (Siemens Medical Solutions USA, Inc.). The mice bearing SKOV3 were injected with  $^{68}\text{Ga}$ -DOTA-MUT-DS (0.28–0.30 MBq [7.6–8.2  $\mu\text{Ci}$ ], 0.46–0.50  $\mu\text{g}$ ) via the tail vein. At different times after injection (30 min, 1 h, and 2 h), the mice were anesthetized with 2% isoflurane and placed prone near the center of the field of view of the scanner. The 5-min static scans were obtained, and the images were reconstructed using a 2-dimensional ordered-subsets expectation maximum algorithm. No background correction was performed. The method for quantification analysis of the images was the same as reported previously (18).

### Western Blot

Tumor lysate was prepared by homogenizing tumor specimens in a radioimmunoprecipitation assay buffer (Sigma). The supernatant was collected by centrifugation at 14,000 rpm for 10 min at  $4^\circ\text{C}$ . The protein concentrations of the samples were measured using the Bradford assay (Bio-Rad). An equal amount of protein from each sample was loaded onto a 10% NuPAGE Bis-Tris gel (Invitrogen) and electroblotted to a polyvinylidene fluoride membrane. After blocking with Tris-buffered saline plus 0.05% polysorbate 20 containing 5% powdered milk, the membrane was incubated with a rabbit monoclonal antihuman *HER2* antibody (Cell Signal Technology) (1:1,000) overnight, followed by incubation with the horseradish peroxidase-conjugated goat antirabbit IgG (Invitrogen) (1:5,000) for 1 h. After extensive washing, the protein bands were visualized using ECL Plus (Invitrogen). For determining the relative *HER2* protein levels, the intensity of the *HER2* protein band was normalized with the intensity of the  $\alpha$ -tubulin (Sigma-Aldrich) band from each sample using Image Processing and Analysis in Java (ImageJ; open-source image software downloaded from <http://rsb.info.nih.gov/ij/>).

### Statistical Methods

Statistical analysis was performed using the Student *t* test for unpaired data. A 95% confidence level was chosen to determine the significance between groups, with  $P < 0.05$  indicating a significant difference.

## RESULTS

### Chemistry and Radiochemistry

The cyclic 2-helix small protein DOTA-MUT-DS was produced through standard solid-phase peptide synthesis and  $\text{I}_2$  oxidation of the 2 homocysteines. The desired

product was purified by preparative HPLC, and the target compound was generally obtained in 10% yield with more than 95% purity. The retention time on analytic HPLC for DOTA-MUT-DS was 19.1 min. The measured molecular weight, 5,136.77, was consistent with the expected molecular weight, 5,136.53 ( $[M+H]^+$ ,  $C_{218}H_{352}N_{69}O_{69}S_3$ ).

DOTA-MUT-DS was then successfully radiolabeled with  $^{68}\text{Ga}$  at  $75^\circ\text{C}$  during a 20-min incubation. Purification of the radiolabeling solution using RP-HPLC afforded  $^{68}\text{Ga}$ -DOTA-MUT-DS with more than 95% radiochemical purity (Fig. 2A) and 35%–56% decay-corrected yield. The retention time for  $^{68}\text{Ga}$ -DOTA-MUT-DS is 19.1 min. Under several HPLC conditions investigated in this study, the separation of  $^{68}\text{Ga}$ -DOTA-MUT-DS and unlabeled DOTA-MUT-DS was not achieved. A modest specific activity of 2.65–3.69 MBq of  $^{68}\text{Ga}$ -DOTA-MUT-DS per nanomole (13.9–19.4  $\mu\text{Ci}/\mu\text{g}$ ) was generally obtained at the end of synthesis. Furthermore,  $^{68}\text{Ga}$ -DOTA-MUT-DS demonstrated good in vitro stability. After 40 min of incubation with mouse serum, more than 90% of the radiolabeled complex was still intact labeled protein (Fig. 2B).

### HER2-Binding Affinity of DOTA-MUT-DS

The binding affinity of DOTA-MUT-DS was determined to be 4.76 nM by surface plasmon resonance using Biacore, which is almost the same as nonmodified MUT-DS (dissociation constant  $[K_D]$ , 5 nM) (20). This result suggested that DOTA conjugation did not alter the binding affinity of the 2-helix protein. It was also observed that this DOTA-MUT-DS displayed a fast “on” rate (association constant,  $1.62 \times 10^5 \text{ s}^{-1}$ ), and slow “off” rate ( $K_D$ ,  $7.7 \times 10^{-4} \text{ s}^{-1}$ ) (Fig. 3).

### In Vitro Cell Assays of $^{68}\text{Ga}$ -DOTA-MUT-DS

The *HER2*-expressing tumor cell line SKOV3 was used for evaluation of the *HER2*-targeting ability of  $^{68}\text{Ga}$ -DOTA-MUT-DS. Cell uptake of the probe at  $37^\circ\text{C}$  over a 2-h incubation period is shown in Figure 4. The probe quickly accumulated in the SKOV3 cells and reached  $1.76\% \pm 0.22\%$  of the applied activity at 0.5 h. The uptake then increased to  $3.19\% \pm 0.31\%$  at 1 h and slightly dropped to  $2.57\% \pm 0.48\%$  at 2 h ( $P > 0.05$ ). When incubated with a large excess of nonradioactive Affibody molecule  $Z_{HER2:477}$ , SKOV3 cells showed significantly

inhibited uptake ( $P < 0.05$ ) at all incubation time points. For example, uptake was only  $0.17\% \pm 0.07\%$  at 1 h of incubation, and uptake was below 0.1% at 2 h of incubation. Overall, these results strongly suggest that  $^{68}\text{Ga}$ -DOTA-MUT-DS has *HER2*-binding specificity.

### In Vivo Biodistribution Studies

The in vivo biodistribution of  $^{68}\text{Ga}$ -DOTA-MUT-DS was examined in a SKOV3 human ovarian tumor-bearing mouse model. Biodistribution of the probe at 0.5, 1, and 2 h was studied (Table 1). A rapid and good accumulation of activity in the *HER2*-expressing SKOV3 tumors was observed at early time points ( $2.55 \pm 0.72 \text{ \%ID/g}$  at 0.5 h after injection). Tumor uptake continually increased to  $4.04 \pm 0.24 \text{ \%ID/g}$  at 2 h after injection. The 2-helix  $^{68}\text{Ga}$ -DOTA-MUT-DS displayed rapid blood clearance: the  $1.78 \pm 0.68 \text{ \%ID/g}$  observed at 0.5 h after injection dropped to  $0.77 \pm 0.2$  and  $0.60 \pm 0.11 \text{ \%ID/g}$  at 1 and 2 h, respectively. Hence, the tumor-to-blood ratio was  $1.59 \pm 0.7$  at 0.5 h, increased to  $5.32 \pm 0.18$  at 1 h, and maximized at  $7.72 \pm 2.1$  at 2 h. The tumor-to-muscle ratio maximized at  $9.94 \pm 1.29$  at 1 h. Of the major organs, the liver uptake was  $1.14 \pm 0.19 \text{ \%ID/g}$  at 0.5 h and gradually decreased to  $0.85 \pm 0.09 \text{ \%ID/g}$  at 2 h. The lung uptake was  $1.76 \pm 0.61 \text{ \%ID/g}$  at 0.5 h and  $0.67 \pm 0.14 \text{ \%ID/g}$  at 2 h. Kidney uptake remained more than 200  $\text{ \%ID/g}$  at all time points. All other major organs examined in this study showed low uptake ( $<1.10 \text{ \%ID/g}$  at 1 h) and fast clearance.

The in vivo tumor-targeting specificity was further evaluated by injection of an Hsp90 inhibitor, 17-DMAG. Pretreatment of tumor mice with 17-DMAG significantly reduced the SKOV3 tumor uptake of  $^{68}\text{Ga}$ -DOTA-MUT-DS to around 32% of the corresponding nontreated tumor uptake at 2 h after injection ( $4.12 \pm 0.83$  vs.  $0.74 \pm 0.23 \text{ \%ID/g}$ ,  $P < 0.01$ ). Consequently, the tumor-to-blood ratio was significantly decreased for the group of mice with 17-DMAG treatment ( $7.72 \pm 2.1$  vs.  $1.69 \pm 0.16$ ,  $P < 0.01$ ). Interestingly, liver and kidney uptake also dropped after 17-DMAG treatment ( $P < 0.05$ ).

### Small-Animal PET

Decay-corrected coronal and transaxial small-animal PET images of a mouse bearing SKOV3 tumor at 0.5, 1,

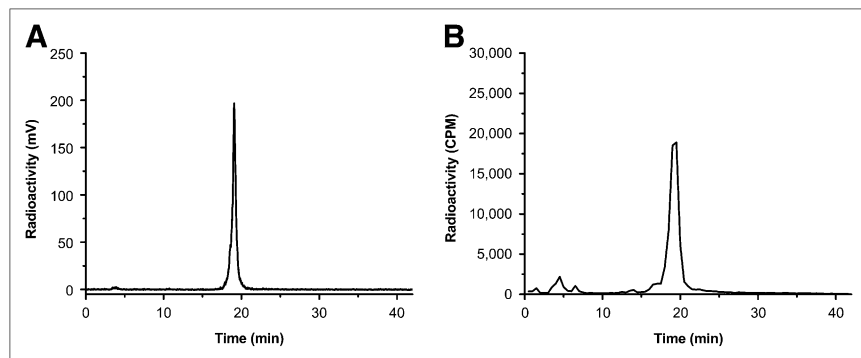


**FIGURE 2.** HPLC radiochromatograms of purified  $^{68}\text{Ga}$ -DOTA-MUT-DS (A) and radiolabeled probe after 40 min of incubation with mouse serum (B).

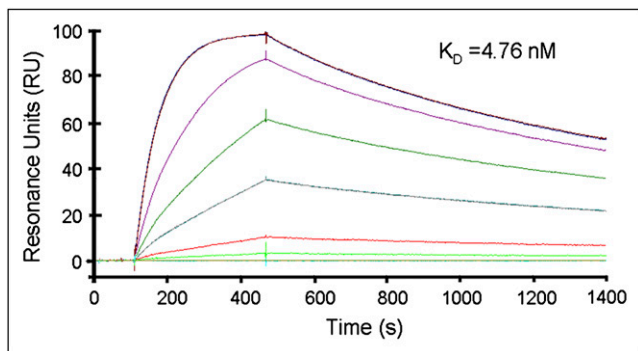


**FIGURE 3.** Biosensor binding studies of DOTA-MUT-DS.

and 2 h after tail vein injection of  $^{68}\text{Ga}$ -DOTA-MUT-DS are shown in Figure 5A. SKOV3 tumors were visible especially at 0.5–2 h after injection, with good tumor-to-background contrast. Also observed was a high accumulation of activity in the kidneys for  $^{68}\text{Ga}$ -DOTA-MUT-DS. For 17-DMAG-treated mice, the tumors were hardly visible on PET images at any time point (Fig. 5B). Quantification analysis of PET images showed much lower uptake for treated mice than for nontreated mice ( $P < 0.01$ ) (Fig. 5C).

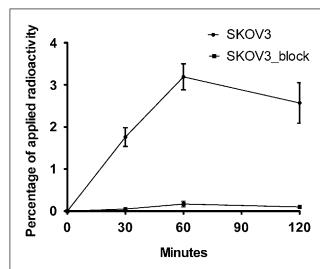
#### Western Blot

Western blot analysis is shown in Figure 6. The *HER2* protein band was detected and band intensity normalized with the  $\alpha$ -tubulin band using ImageJ software. The ratios for SKOV3 tumor to tubulin were  $1.17 \pm 0.3$  and  $0.32 \pm 0.06$  for nontreated tumor mice and 17-DMAG-treated mice, respectively. *HER2* expression was downregulated by 72%.

#### DISCUSSION

Only a few Food and Drug Administration–approved imaging agents are available for clinical cancer imaging. Although different *HER2* PET techniques have been evaluated in preclinical small-animal tumor models, the development of a PET probe for routine clinical use has not yet been successful, mainly because of the limited *HER2*-binding ligands available to the molecular imaging field. Indeed, most of the effort in developing a *HER2* imaging agent has focused on using *HER2*-avid antibodies or antibody-derived fragments (21,22). Unfortunately, the slow

**FIGURE 4.** Cell uptake of  $^{68}\text{Ga}$ -DOTA-MUT-DS in SKOV3 cells over time at 37°C with or without non-radioactive Affibody molecule  $Z_{\text{HER2}:477}$ . All results are expressed as mean of triplicate measurement  $\pm$  SD.



tumor targeting and normal-tissue clearance of antibody-based probes severely hamper their application in the clinic. Moreover, the poor pharmacokinetic clearance of antibody-based probes generally leads to the selection of radioisotopes with a relatively long half-life, such as  $^{64}\text{Cu}$  (12.7 h),  $^{86}\text{Y}$  (14.7 h),  $^{76}\text{Br}$  (16.2 h), and  $^{124}\text{I}$  (4.18 d), as radiolabels, potentially resulting in an elevated radiation dose to patients (23,24). In addition, good tumor-to-background contrast can be achieved only long after administration of the probe. The limited availability and high cost of these radioisotopes also become significant problems and hinder the further development of antibody-based *HER2* imaging agents. Recently, the rapid progress in protein display technologies has led to the discovery of many small proteins and peptides with high affinity and specificity for a variety of molecular targets (1,25,26). Among these small proteins, 3-helix Affibody molecules have been demonstrated to be excellent platforms for imaging agent development. Besides high affinity and stability, their relatively small size generally leads to fast clearance and tumor accumulation and a relatively short in vivo biologic half-life, which potentially matches well with the clinically relevant short physical half-life of radioisotopes such as  $^{18}\text{F}$ ,  $^{68}\text{Ga}$ , and  $^{99\text{m}}\text{Tc}$  (3,4,14,17,27–31).

Clearly, the size of biologic molecules is an important parameter in PET probe development. Can even smaller Affibody molecules with high binding affinity retain specific tumor-targeting ability while gaining preferential in vivo properties? In this study, a 2-helix small protein, DOTA-MUT-DS (~4.6 kDa, 39 amino acid residues), two thirds the size of the smallest Affibody, for the first time was labeled with  $^{68}\text{Ga}$  and evaluated in vivo for PET imaging of *HER2*. Besides good stability and specific tumor-targeting ability, especially when compared with 3-helix Affibody molecules, the potential advantages expected for smaller 2-helix constructs include the possibility of facile synthetic generation, easier library generation for screening, economic viability, potentially lower immunogenic potential, faster extravasation, earlier tumor accumulation, and reasonable tumor retention.

DOTA-MUT-DS was successfully synthesized through standard solid-phase peptide synthesis and  $\text{I}_2$  oxidation of the 2 homocysteines. Biacore results demonstrated that the binding affinity of DOTA-MUT-DS was 4.76 nM, which was on the order of 2-fold lower than that of its 3-helix counterpart,  $Z_{\text{HER2}:342}$  ( $K_D$ , 22 pM) (3). However, because the single-digit nanomolar binding affinity is still a respectable value, we felt encouraged to radiolabel the peptide and further evaluate the probe in vivo. The radiolabeling was performed under mild conditions (pH 4.5, 75°C, 20 min). Incubation of  $^{68}\text{Ga}$ -DOTA-MUT-DS with mouse serum demonstrated that the 2-helix protein was stable and thus could be used to follow tumor biodistribution and for imaging studies (Fig. 2B).

The production of the positron-emitting radionuclide  $^{68}\text{Ga}$  does not require a cyclotron on site, making the

**TABLE 1.** Biodistribution Results for  $^{68}\text{Ga}$ -DOTA-MUT-DS in Nude Mice Bearing Subcutaneously Xenotransplanted SKOV3 Human Ovarian Cancer

Site	0.5 h	1 h	2 h	2-h block
Tumor	2.55 ± 0.72	4.04 ± 0.24	4.12 ± 0.83*	0.74 ± 0.23
Blood	1.78 ± 0.68	0.77 ± 0.02	0.60 ± 0.11	0.49 ± 0.14
Heart	0.73 ± 0.17	0.30 ± 0.09	0.21 ± 0.05	0.15 ± 0.04
Liver	1.14 ± 0.19	1.08 ± 0.08	0.85 ± 0.09*	0.26 ± 0.12
Lung	1.76 ± 0.61	0.98 ± 0.05	0.67 ± 0.14	0.49 ± 0.10
Muscle	0.86 ± 0.20	0.54 ± 0.24	0.69 ± 0.29	0.38 ± 0.09
Spleen	1.21 ± 0.27	1.08 ± 0.20	0.80 ± 0.25	0.51 ± 0.23
Brain	0.23 ± 0.08	0.17 ± 0.06	0.14 ± 0.03	0.08 ± 0.04
Intestine	0.58 ± 0.18	0.39 ± 0.07	0.37 ± 0.09	0.24 ± 0.16
Skin	0.65 ± 0.02	0.58 ± 0.03	0.39 ± 0.15	0.25 ± 0.09
Stomach	0.58 ± 0.31	0.43 ± 0.14	0.17 ± 0.05	0.12 ± 0.02
Pancreas	0.43 ± 0.20	0.32 ± 0.08	0.17 ± 0.05	0.08 ± 0.03
Bone	0.49 ± 0.19	0.47 ± 0.07	0.31 ± 0.08	0.19 ± 0.13
Kidney	208.44 ± 99.21	281.99 ± 35.64	228.92 ± 21.75*	112.10 ± 59.66
Tumor-to-blood ratio	1.59 ± 0.70	5.32 ± 0.18	7.72 ± 2.10	1.69 ± 0.16
Tumor-to-muscle ratio	3.09 ± 1.27	9.94 ± 1.29	5.40 ± 1.11	2.34 ± 1.36

\* $P < 0.05$ , compared with 2-h block.

Data are %ID/g after intravenous injection of probe (296 kBq [8  $\mu\text{Ci}$ ]) at 0.5, 1, and 2 h ( $n = 3$ ). For 2-h block, mice were treated with 17-DMAG for 24 h and then injected with  $^{68}\text{Ga}$ -DOTA-MUT-DS.

approach feasible to more clinicians and researchers. Considering the short half-life of  $^{68}\text{Ga}$ , our biodistribution and imaging data were acquired in a relatively short time frame ( $\leq 2$  h after injection). This could also be more appealing to clinical practice. Consistent with our expectation, the tumor uptake, ratios of tumor to normal tissue, and tumor imaging quality were good because of the good tumor-targeting ability and fast clearance from normal organs (Table 1). As early as 0.5 h after injection, the tumor uptake was already  $2.55 \pm 0.72$  %ID/g, and it continued to increase to  $4.12 \pm 0.83$  %ID/g at 2 h after injection. From 1 to 2 h after injection, tumor uptake remained at around 4 %ID/g, with no statistical difference between these 2 time points ( $P > 0.05$ ). At the same time, the radioactivity in blood and most major organs was largely cleared within 2 h after injection, resulting in a continual rise in tumor-to-normal tissue ratios. The demonstrated fast tumor uptake and reasonable tumor

retention of  $^{68}\text{Ga}$ -DOTA-MUT-DS in *HER2*-expressing tumors potentially enable clinicians to obtain *HER2* PET images with improved contrast within a reasonable time frame. Liver uptake remained at around 1 %ID/g at both 30 min and 1 h after injection—a much lower value than for its  $^{64}\text{Cu}$ -labeled 3-helix counterpart (Gang Ren et al., unpublished data, May 2008). For example, at 1 h after injection, liver uptake was only  $1.08 \pm 0.08$  %ID/g for  $^{68}\text{Ga}$ -DOTA-MUT-DS but was around  $5.24 \pm 0.82$  %ID/g for 3-helix  $^{64}\text{Cu}$ -DOTA-*Z*<sub>HER2:477</sub> ( $P < 0.05$ ). The lower liver uptake may be attributed to the lower negative charge of  $^{68}\text{Ga}$ -DOTA-MUT-DS, leading to a reduction in the affinity of the radiometal metabolite for hepatic scavenger receptors. Additionally, different lipophilicities of the probes, different stabilities of the DOTA chelator with  $^{64}\text{Cu}$  and  $^{68}\text{Ga}$ , and different intracellular behaviors may also play important roles in lower liver uptake for  $^{68}\text{Ga}$ -MUT-DS.

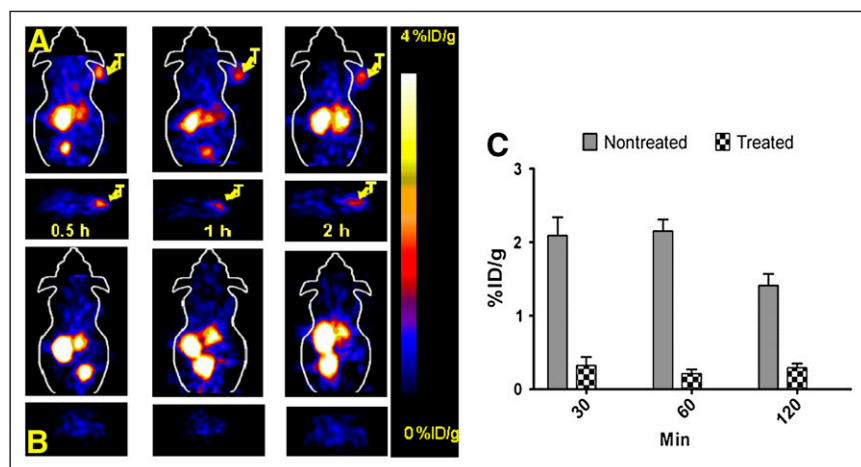


**FIGURE 5.** Representative decay-corrected coronal (top) and transaxial (bottom) PET images of nude mice bearing SKOV3 tumor on right shoulder at 0.5, 1, and 2 h after tail vein injection of  $^{68}\text{Ga}$ -DOTA-MUT-DS: nontreated group (A) and treated group (B) (images were acquired after 24 h of treatment with 17-DMAG; arrows indicate location of tumors). (C) Quantification analysis of tumor uptake before and after 17-DMAG treatment. Data are expressed as mean of 3 mice  $\pm$  SD.

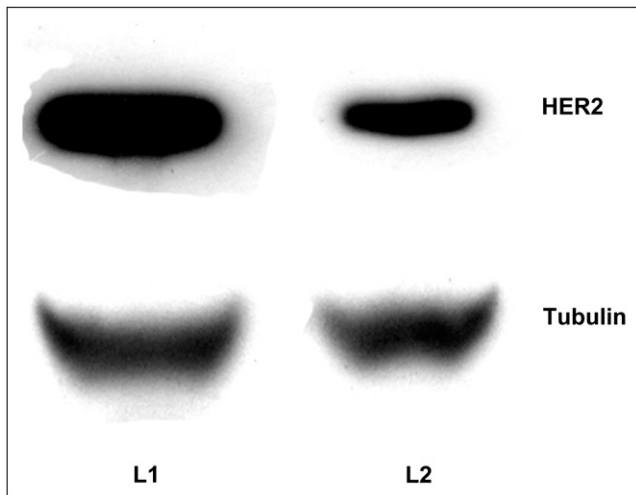


**FIGURE 6.** Representative Western blot detection of *HER2* expression in tumor tissue samples. SKOV3 tumor homogenates were prepared and 50  $\mu\text{g}$  of protein were detected with rabbit antihuman *HER2* monoclonal antibody. L1 = lane 1, nontreated tumor; L2 = lane 2, tumor treated with 17-DMAG.

Kidney uptake was quite high for  $^{68}\text{Ga}$ -DOTA-MUT-DS (208.44  $\pm$  99.21 %ID/g at 30 min and 281.99  $\pm$  35.64 %ID/g at 1 h). Clearly,  $^{68}\text{Ga}$ -DOTA-MUT-DS is not suitable for detecting lesions in the urinary system and its adjacent organs. Because the kidney is not a common site for breast cancer metastases, the high kidney uptake of the probe may not be a major concern for diagnostic purposes. If DOTA-MUT-DS is further developed for radiotherapeutic application, dosimetry studies should be performed to address the toxicity to the kidneys, considering that the kidney is a radiosensitive organ. Different strategies such as the administration of cationic amino acids, modification of amino acids, changing of radiolabeling, and use of cleavable linkers may be applied to potentially reduce uptake by the kidneys (31,32).

The specificity of  $^{68}\text{Ga}$ -DOTA-MUT-DS was tested both in vitro and in vivo. The in vitro specificity of  $^{68}\text{Ga}$ -DOTA-MUT-DS was confirmed by the use of an excess of nonradiolabeled  $Z_{\text{HER2}:477}$  in cell cultures. Coincubation of  $Z_{\text{HER2}:477}$  inhibited cellular uptake of  $^{68}\text{Ga}$ -DOTA-MUT-DS by more than 80% at 0.5 h and later, suggesting that cellular uptake was specific. In live animals, reports indicate that geldanamycin inhibits *HER2* signaling by binding to an Hsp90 chaperone protein, which further induces proteasomal degradation (22,33). 17-DMAG, an Hsp90 inhibitor and an analog of geldanamycin, was thus used for modulation of *HER2* expression, as was evidenced by Western blot studies (Fig. 6). The in vivo specificity of  $^{68}\text{Ga}$ -DOTA-MUT-DS was then tested by pretreatment of tumor-bearing mice with 17-DMAG. For small-animal PET, excellent tumor-to-background contrast was obtained at 0.5, 1, and 2 h after injection for nontreated animals (Fig.

5A) whereas the SKOV3 tumors in the treated group could barely be seen (Fig. 5B). Quantification analysis of PET images suggested that the accumulated radioactivity in tumor had been reduced by 80% at 2 h after injection (Fig. 5C). Biodistribution studies revealed that the uptake for treated tumors was inhibited by about 68% at 2 h after injection (Table 1). On Western blot studies, the protein expression level was downregulated by about 72% with 17-DMAG treatment, calculated from normalized band intensity (Fig. 6), which was consistent with other reports (22) and correlates well with both ex vivo biodistribution and in vivo imaging results. Interestingly, differences in the uptake of  $^{68}\text{Ga}$ -DOTA-DUT-MS were also observed in liver and kidney in mice with or without 17-DMAG treatment. The reasons for this observation are not yet clear. It seems that 17-DMAG affects clearance of the  $^{68}\text{Ga}$ -labeled protein. More studies are needed to explain this observation.

$^{18}\text{F}$ -FDG has been used extensively in clinical cancer imaging, but its tumor uptake is attributed to glucose transporter 1 and hexokinase expression. Clinical PET studies show that  $^{18}\text{F}$ -FDG has limited value in breast cancer staging and prognosis (34,35). More important,  $^{18}\text{F}$ -FDG does not provide any information about *HER2* status in patients. In contrast, *HER2*-targeted PET probes such as  $^{68}\text{Ga}$ -MUT-DS may provide a useful tool for imaging patients' *HER2* expression noninvasively. It is expected that  $^{68}\text{Ga}$ -MUT-DS will find important applications in the clinical management of breast cancer patients. The *HER2* PET probe can potentially be used for several purposes, such as to stratify patients for *HER2*-targeted treatment, monitor the efficacy of *HER2* treatment, and determine the prognosis of patients based on their *HER2* expression.

Compared with many of the reported radiolabeled anti-*HER2* 3-helix Affibody molecules ( $Z_{\text{HER2}:342}$  and  $Z_{\text{HER2}:477}$ ),  $^{68}\text{Ga}$ -DOTA-MUT-DS has a lower absolute tumor uptake, probably because of the modest specific activity and relatively low *HER2*-binding affinity (nM vs. pM) of the probe (3). Reasonably specific activity is needed for a probe for receptor-based PET imaging of tumors. Although the specific activity of  $^{68}\text{Ga}$ -DOTA-MUT-DS achieved in this study was moderate, it is comparable to that of the  $^{111}\text{In}$ -labeled 3-helix Affibody that was successfully used for imaging small tumor metastases (diameter, 12–14 mm; 5.8 g) in patients (36). This result suggests that our method is clinically relevant for the preparation of  $^{68}\text{Ga}$ -DOTA-MUT-DS. With further optimizations such as modifications of labeling conditions and the use of different  $^{68}\text{Ga}$  chelators, such as NOTA (37,38), we may further improve the specific activity of the probe. Finally, excellent in vivo PET imaging of tumors in small animals has been achieved with  $^{68}\text{Ga}$ -DOTA-MUT-DS, demonstrating the great potential of the 2-helix protein as a platform for molecular imaging of tumor targets. The high abundance of positrons (89%) and short half-life of  $^{68}\text{Ga}$  also make repetitively high-quality PET acquisitions possible.  $^{68}\text{Ga}$ -

DOTA-MUT-DS may also be useful for the noninvasive monitoring of *HER2*-targeted therapeutic efficacy in research and, potentially, clinical settings.

## CONCLUSION

A 2-helix anti-*HER2* small protein, DOTA-MUT-DS, has been successfully synthesized and radiolabeled with  $^{68}\text{Ga}$  for molecular imaging of *HER2* in vivo. Biodistribution and small-animal PET studies further demonstrated that 2-helix  $^{68}\text{Ga}$ -DOTA-MUT-DS is a promising PET probe for imaging *HER2* receptor expression in living mice. This proof-of-concept research established the feasibility of using a 2-helix protein scaffold for in vivo imaging of tumor biomarkers. The 2-helix protein scaffold represents a novel, attractive platform for cancer targeting.

## ACKNOWLEDGMENTS

This work was supported, in part, by Medical Diagnostics, GE Healthcare, grant R24 CA93862 from the National Cancer Institute (NCI) Small Animal Imaging Resource Program (SAIRP), California Breast Cancer Research Program 14IB-0091, and an SNM pilot research grant. We thank Dr. Joshua Hoerner and Hans Grade of GE Global Research for mass spectrometer analysis and Dr. Alex Gibson of GE Healthcare for helpful suggestions and for reviewing the manuscript.

## REFERENCES

- Nygren PA. Alternative binding proteins: affibody binding proteins developed from a small three-helix bundle scaffold. *FEBS J.* 2008;275:2668–2676.
- Nygren PA, Skerra A. Binding proteins from alternative scaffolds. *J Immunol Methods.* 2004;290:3–28.
- Orlova A, Magnusson M, Eriksson TL, et al. Tumor imaging using a picomolar affinity *HER2* binding affibody molecule. *Cancer Res.* 2006;66:4339–4348.
- Orlova A, Tolmachev V, Pehrson R, et al. Synthetic affibody molecules: a novel class of affinity ligands for molecular imaging of *HER2*-expressing malignant tumors. *Cancer Res.* 2007;67:2178–2186.
- Nordberg E, Orlova A, Friedman M, et al. In vivo and in vitro uptake of  $^{111}\text{In}$ , delivered with the affibody molecule ( $\text{Z}_{\text{EGFR},955}$ )<sub>2</sub>, in EGFR expressing tumour cells. *Oncol Rep.* 2008;19:853–857.
- Tolmachev V, Friedman M, Sandstrom M, et al. Affibody molecules for epidermal growth factor receptor targeting in vivo: aspects of dimerization and labeling chemistry. *J Nucl Med.* 2009;50:274–283.
- Jonsson A, Dogan J, Herne N, Abrahmsen L, Nygren PA. Engineering of a femtomolar affinity binding protein to human serum albumin. *Protein Eng Des Sel.* 2008;21:515–527.
- Gronwall C, Snelders E, Palm AJ, Eriksson F, Herne N, Stahl S. Generation of Affibody ligands binding interleukin-2 receptor alpha/CD25. *Biotechnol Appl Biochem.* 2008;50:97–112.
- Lundberg E, Brismar H, Graslund T. Selection and characterization of Affibody ligands to the transcription factor c-Jun. *Biotechnol Appl Biochem.* 2009;52:17–27.
- Gronwall C, Jonsson A, Lindstrom S, Gunneriusson E, Stahl S, Herne N. Selection and characterization of Affibody ligands binding to Alzheimer amyloid beta peptides. *J Biotechnol.* 2007;128:162–183.
- Wikman M, Rowcliffe E, Friedman M, et al. Selection and characterization of an HIV-1 gp120-binding affibody ligand. *Biotechnol Appl Biochem.* 2006;45:93–105.
- Tolmachev V, Nilsson FY, Widstrom C, et al.  $^{111}\text{In}$ -benzyl-DTPA- $\text{Z}_{\text{HER2},342}$ , an affibody-based conjugate for in vivo imaging of *HER2* expression in malignant tumors. *J Nucl Med.* 2006;47:846–853.
- Kramer-Marek G, Kiesewetter DO, Martiniova L, Jagoda E, Lee SB, Capala J. [ $^{18}\text{F}$ ]FBEM- $\text{Z}_{\text{HER2},342}$ -Affibody molecule: a new molecular tracer for in vivo monitoring of *HER2* expression by positron emission tomography. *Eur J Nucl Med Mol Imaging.* 2008;35:1008–1018.
- Tran T, Engfeldt T, Orlova A, et al. In vivo evaluation of cysteine-based chelators for attachment of  $^{99\text{m}}\text{Tc}$  to tumor-targeting Affibody molecules. *Bioconjug Chem.* 2007;18:549–558.
- Nilsson FY, Tolmachev V. Affibody molecules: new protein domains for molecular imaging and targeted tumor therapy. *Curr Opin Drug Discov Devel.* 2007;10:167–175.
- Steffen AC, Almqvist Y, Chyan MK, et al. Biodistribution of  $^{211}\text{At}$  labeled *HER2* binding affibody molecules in mice. *Oncol Rep.* 2007;17:1141–1147.
- Fortin MA, Orlova A, Malmstrom PU, Tolmachev V. Labelling chemistry and characterization of [ $^{90}\text{Y}/^{177}\text{Lu}$ ]-DOTA- $\text{Z}_{\text{HER2},342,3}$  Affibody molecule, a candidate agent for locoregional treatment of urinary bladder carcinoma. *Int J Mol Med.* 2007;19:285–291.
- Cheng Z, De Jesus OP, Namavari M, et al. Small-animal PET imaging of human epidermal growth factor receptor type 2 expression with site-specific  $^{18}\text{F}$ -labeled protein scaffold molecules. *J Nucl Med.* 2008;49:804–813.
- Lee SB, Hassan M, Fisher R, et al. Affibody molecules for in vivo characterization of *HER2*-positive tumors by near-infrared imaging. *Clin Cancer Res.* 2008;14:3840–3849.
- Webster JMZR, Gambhir SS, Cheng Z, Syud FA. Engineered two-helix small proteins for molecular recognition. *Chembiochem.* 2009;10:1293–1296.
- Tang Y, Wang J, Scollard D, et al. Imaging of *HER2*/neu-positive BT-474 human breast cancer xenografts in athymic mice using  $^{111}\text{In}$ -trastuzumab (Herceptin) Fab fragments. *Nucl Med Biol.* 2005;32:51–58.
- Smith-Jones PM, Solit DB, Akhurst T, Afroze F, Rosen N, Larson SM. Imaging the pharmacodynamics of *HER2* degradation in response to Hsp90 inhibitors. *Nat Biotechnol.* 2004;22:701–706.
- Holliger P, Hudson PJ. Engineered antibody fragments and the rise of single domains. *Nat Biotechnol.* 2005;23:1126–1136.
- Loo L, Robinson MK, Adams GP. Antibody engineering principles and applications. *Cancer J.* 2008;14:149–153.
- Uchiyama F, Tanaka Y, Minari Y, Tokui N. Designing scaffolds of peptides for phage display libraries. *J Biosci Bioeng.* 2005;99:448–456.
- Rothe A, Hosse RJ, Power BE. In vitro display technologies reveal novel biopharmaceutics. *FASEB J.* 2006;20:1599–1610.
- Orlova A, Nilsson FY, Wikman M, et al. Comparative in vivo evaluation of technetium and iodine labels on an anti-*HER2* affibody for single-photon imaging of *HER2* expression in tumors. *J Nucl Med.* 2006;47:512–519.
- Namavari M, Padilla De Jesus O, Cheng Z, et al. Direct site-specific radiolabeling of an affibody protein with 4- $^{18}\text{F}$ fluorobenzaldehyde via oxime chemistry. *Mol Imaging Biol.* 2008;10:177–181.
- Orlova A, Rosik D, Sandstrom M, Lundqvist H, Einarsson L, Tolmachev V. Evaluation of [ $^{111/114\text{m}}\text{In}$ ]CHX-A"-DTPA- $\text{Z}_{\text{HER2},342}$ , an affibody ligand conjugate for targeting of *HER2*-expressing malignant tumors. *Q J Nucl Med Mol Imaging.* 2007;51:314–323.
- Ahlgren S, Orlova A, Rosik D, et al. Evaluation of maleimide derivative of DOTA for site-specific labeling of recombinant affibody molecules. *Bioconjug Chem.* 2008;19:235–243.
- Tolmachev V, Orlova A, Pehrson R, et al. Radionuclide therapy of *HER2*-positive microxenografts using a  $^{177}\text{Lu}$ -labeled *HER2*-specific Affibody molecule. *Cancer Res.* 2007;67:2773–2782.
- Gotthardt M, van Eerd-Vismale J, Oyen WJ, et al. Indication for different mechanisms of kidney uptake of radiolabeled peptides. *J Nucl Med.* 2007;48:596–601.
- Smith-Jones PM, Solit D, Afroze F, Rosen N, Larson SM. Early tumor response to Hsp90 therapy using *HER2* PET: comparison with  $^{18}\text{F}$ -FDG PET. *J Nucl Med.* 2006;47:793–796.
- Rosen EL, Eubank WB, Mankoff DA. FDG PET, PET/CT, and breast cancer imaging. *Radiographics.* 2007;27(suppl 1):S215–S229.
- Shimoda W, Hayashi M, Murakami K, Oyama T, Sunagawa M. The relationship between FDG uptake in PET scans and biological behavior in breast cancer. *Breast Cancer.* 2007;14:260–268.
- Baum R, Orlova A, Tolmachev V, Feldwisch J. Receptor PET/CT and SPECT using an Affibody molecule for targeting and molecular imaging of *HER2* positive cancer in animal xenografts and human breast cancer patients [abstract]. *J Nucl Med.* 2006;47(suppl):108P.
- Li ZB, Chen K, Chen X.  $^{68}\text{Ga}$ -labeled multimeric RGD peptides for microPET imaging of integrin  $\alpha_v\beta_3$  expression. *Eur J Nucl Med Mol Imaging.* 2008;35:1100–1108.
- Zhernosekov KP, Filosofov DV, Baum RP, et al. Processing of generator-produced  $^{68}\text{Ga}$  for medical application. *J Nucl Med.* 2007;48:1741–1748.